Parametrising a Model of Clinopyroxene/Melt Partition Coefficients for Sodium to Higher Upper Mantle Pressures

Julia Marleen Schmidt
Institute of Geological Sciences)
Freie Universität Berlin
Berlin, Germany
email: julia.schmidt@fu-berlin.de

Lena Noack
Institute of Geological Sciences
Freie Universität Berlin
Berlin, Germany
email: lena.noack@fu-berlin.de

***Abstract*—Mineral/melt partition coefficients describe the redistribution of trace elements during melting processes. They are highly influenced by changing pressure, temperature, and composition. We find that for sodium, partition coefficients rise in the order of two magnitudes from 0-15 GPa along the peridotite solidus temperature. Still, because of lacking high-pressure experimental data and the limited pressure range of most partitioning models, mantle and crust evolution models normally rely on constant partition coefficients. Based on an earlier model, we created a thermodynamic model which calculates sodium partition coefficients between clinoproxene and anhydrous silicate melts. With the results, we parametrise an equation over 0-15 GPa and various melt fractions. Our new parametrised partitioning model for sodium complements previous models and is applicable up to the mantle transition zone (4-12 GPa/1850-2360 K). Knowing the sodium partitioning behavior enables us to base further calculations for many other elements on it.**

***Keywords*—partition coefficients; thermodynamic modelling**

I. INTRODUCTION

Inside the Earth and other terrestrial planets, partial melts usually control the redistribution of trace elements from the mantle to the crust. If melt is buoyant due to a lower density than the surrounding rock, it moves upwards and transports the previously incorporated incompatible trace elements towards the surface. This leads to enriched reservoirs near the surface and depleted upper mantle areas. Expanding the redistribution concept to a certain number of elements leads to the creation of trace element patterns, which are unique geochemical markers of the events that led to the exact appearance and compositions of a rock of interest [1][2][3].

During melting, partition coefficients describe if an element prefers to be incorporated into a mineral or, if it is incompatible, into melt. Partitioning data for peridotite including the minerals olivine, orthopyroxene, and clinopyroxene show that in mantle rocks, clinopyroxene is the mineral taking in most incompatible trace elements [4][5]. This makes clinopyroxene the mineral with the largest influence on trace element redistribution.

Since partition coefficients of sodium between clinopyroxene and silicate melt are highly affected by changing pressure and temperature, partition coefficient models should consider these parameters. Because of analytical limitations, there are only few measured partition coefficients available for high-pressure conditions. Additionally, partition coefficient models are often only applicable for rather low pressures. This is the reason why so far, partial melt simulations in some mantle evolution models either neglected partition coefficients and chose pre-defined elemental abundances in mantle melts [6], or settled for constant experimentally derived and estimated partition coefficients [7][8][9][10].

In 1937, Goldschmidt postulated that both the matching size and charge of the mineral's lattice site and element of interest determine an element's ability to partition into a mineral [11]. This leads to the assumption that not only it is possible to determine the P-T sensitive partition coefficients experimentally, but also by means of numerical modelling. Based on a model of Brice (1975) [12], Blundy et al. (1995) [13] developed a quantitative model and determined a parametrised fit function for clinopyroxene/melt partition coefficients for sodium in the range of 0-4 GPa and 1000-1800°C.

As is shown in Figure 1, partition coefficients of trace elements have a parabolic relationship in an Onuma diagram. The parabolas' curves change in broadness and shift along the x-axis depending on the bulk modulus E and the ideal lattice site radius r_0, respectively. Because of this relationship, it is possible to calculate other trace elements' partition coefficients based on the reference coefficient D_{Na}.

The aim of this study is to implement a thermodynamic model for $D_{Na}^{cpx/melt}$ for a large range of pressures suitable for mantle melt simulations. Furthermore, we parametrise a fit function from the mentioned model that is applicable for upper mantle pressures. This will open the possibility to include partition coefficients depending on pressure and temperature into mantle evolution models and to acquire more realistic model results [14].

The rest of the paper is organized as follows. In section II, we describe the methods used for our parametrisation and thermodynamic model in the appropriate subsections. Section III

 ISBN: 978-1-61208-871-6

is dedicated to the results for the thermodynamic model and parametrisation respectively. Section IV discusses the results and compares them to experimental data. Section V concludes the paper, summarizes the findings, and points out what can be done in future works.

II. METHODS

A. Thermodynamic Model

To obtain the most realistic trace element partitioning results for mantle melting processes, it is useful to determine a strain-compensated partition coefficient D_0 [15]. Strain-compensation means that the redistributed element has the same charge and size as the regular element on the lattice site of the crystal [12]. Therefore, it is assumed that the radius of the element of interest r_i equals the lattice site radius r_0. This way the partition coefficient D_i can be calculated with the following equation:

$$D_i = D_0 \exp\left(\frac{-4\pi E_{M2} N_A (\frac{r_0}{2}(r_i - r_0)^2 + \frac{1}{3}(r_i - r_0)^3)}{RT}\right), \quad (1)$$

where E_{M2} is the bulk modulus of the M2 lattice site, N_A the Avogadro's number, R the gas constant and T the temperature. Here, the lattice site of interest is the crystallographic M2 site of clinopyroxene. Sodium is used as the strain-compensated partition coefficient D_0 because it is the 1+ charge element that has a radius r_i which is closest to the M2 lattice site radius r_0. Therefore, we assume D_0 = D_{Na}.

To calculate the strain-compensated partition coefficient D_0, we took a thermodynamic approach described by Blundy et al. (1995) [13]. For this, we used the melting curve of jadeite and linked it to the activity of jadeite's components in the melt. To calculate the partition coefficients of sodium between clinopyroxene and silicate melt, jadeite was the clinopyroxene of choice because of both, its high concentration in sodium and its ability to mix nearly ideally with diopside [16] and enstatite.

Generally, partition coefficients are given as the weight fraction ratio

$$D_i = \frac{X_i^{crystal}}{X_i^{melt}}, \quad (2)$$

with X_i being the weight percentage of the given component. However, since we obtain partition coefficients with the help of thermodynamic properties, we calculate molar partition coefficients. Based on experiments on plagioclase/fluid partitioning [17], it is broadly assumed that also for other minerals molar partition coefficients nearly equal weight percentage coefficients [18]. Thus, we can make use of Flood's equation for exchange equilibria in molten salts [19]:

$$RT\ lnK_f = \sum N_i \Delta G^0, \quad (3)$$

where K_f is the molar equilibrium constant, N_i the concentration of the component and ΔG^0 the Gibbs' free energy of change. Because we use a thermodynamic approach for our calculations, N_i can be neglected and is set to one. The molar

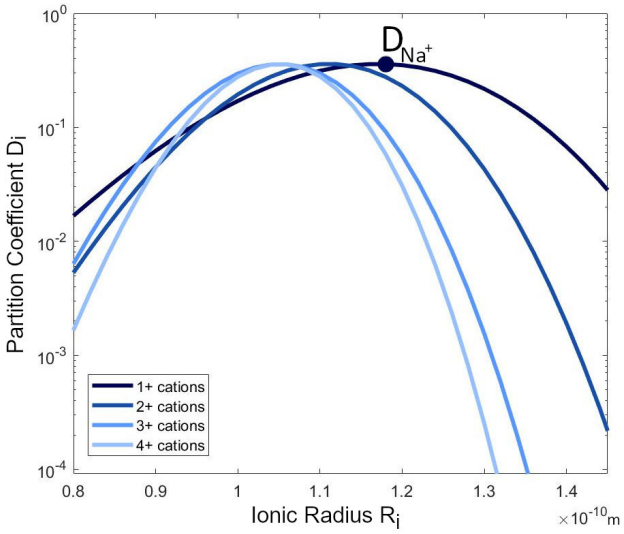

Figure 1. Partition coefficients of 1+ to 4+ charged cations in the clinopyroxene M2 lattice site. Modelled after Wood et al. (1997) [18]. Here, D_{Na} equals D_0.

partitioning of jadeite D^{jd} can be expressed by using K_f in the expression

$$D_{jd} = \frac{1}{K_f} = \frac{a_{jd}^{cpx}}{a_{jd}^{melt}}, \quad (4)$$

where a_{jd}^{cpx} and a^{melt} are the mole of the solid clinopyroxene and molten components, respectively. Here, we assume an ideal case where the activity equals the mole fraction of the elements of interest. Thus, we assume $a_{jd}^{cpx} = X_{Na}^{cpx}$ and $a_{jd}^{melt} = X_{Na}^{melt}$. Taking (4) and rearranging (3) leads to the following equation:

$$D_{Na}^{cpx/melt} = \exp\left(\frac{\Delta G_{f(P,T)}}{RT}\right). \quad (5)$$

Besides (5), one more equation is needed to determine D_{Na} thermodynamically. Equation (6) relates the entropy of the melting reaction to its heat capacity and melting point T_f of jadeite at the pressure P_f=0.0001 GPa. By including the enthalpy, we determine the Gibb's free energy change of reaction with the following equation:

$$\begin{aligned}\Delta G_{(f(P,T))} =& \Delta H_{f(P_f,T_f)} + \int_{T_f}^{T} \Delta C_p dT \\ & - T\left(\Delta S_{f(P_f,T_f)} \right. \\ & \left. + \int_{T_f}^{T} \frac{\Delta C_p}{T} dT\right) + \int_{P_f}^{P} \Delta V_{f(T)} dP, \end{aligned} \quad (6)$$

where $\Delta H_{(f(P_f,T_f)}$ is the entropy, $\Delta S_{f(P_f,T_f)}$ the enthalpy and ΔC_p the difference between the local P,T values and P_f,T_f. $\Delta V_{f(T)}$ is the molar volume of fusion at pressure P_f extrapolated to the temperature of interest [13]. We calculate D_{Na} by inserting (6) into (5).

To be able to solve (6), we use the Maier-Kelly power function [20] to calculate the heat capacity C_p (as stated in

Table I). With the given parameters we can solve the first two integrals in (6) analytically, by evaluating the heat capacity of the solid at temperature T and the melt heat capacity at T_f. To solve the third part of the integral in (6) we use a Riemann integral, where we approximate the intervals on subintervals defined over a pressure vector of n=1000 steps from P=0.0001 to 15 GPa and assume that the volumes of melt and solid are constant in each subinterval.

$$\begin{aligned}\int_{P_f}^{P} \Delta V_{f(T)} dP = & \sum_{i=1}^{n-1} \int_{P_i}^{P_{i+1}} \Delta V_{f(T),i} dP \\ \approx & \sum_{i=1}^{n-1} \Delta V_{f(T),i} \int_{P_i}^{P_{i+1}} dP \\ = & \sum_{i=1}^{n-1} \Delta V_{f(T),i} \left(P_{i+1} - P_i\right) \end{aligned} \quad (7)$$

where $\Delta V_{f(T),i}$ is the volume of fusion, i.e., the volume difference between melt and solids. The calculation of V_{solid} and V_{melt} is done separately using an isothermal Birch-Murnaghan equation of state:

$$P = 1.5 K_T \left(x^{\frac{7}{3}} - x^{\frac{5}{3}}\right) \left(1 + 0.75(K' - 4)\left(x^{\frac{2}{3}} - 1\right)\right), \quad (8)$$

where $x = V^0/V$. K_T is the bulk modulus for pyroxene and K' its derivative. The volumes further depend on temperature via

$$V(T) = V \cdot \exp\left(\int_{T_0}^{T} \alpha(T) dT\right). \quad (9)$$

Here, we assume that the thermal expansion coefficient α is constant for melts and solids (see Table I), hence

$$\begin{aligned}\Delta V_{f(T),i} = & \\ & V_{melt}(P_i) \cdot \exp\left(\alpha^0_{melt}(T - T_f)\right) \\ & - V_{solid}(P_i) \cdot \exp\left(\alpha^0_{solid}(T - T_0)\right). \end{aligned} \quad (10)$$

T_0 is set to 298 K. The partition coefficient D_{Na} is then derived for varied pressures and temperatures by inserting ΔG into (5).

B. Fit Function Development

The thermodynamic model indicates that partition coefficients are not only dependent on pressure, but temperatures and therefore melt fractions as well. Thus, to develop a mantle melt fit function for the reference coefficient D_{Na}, we calculated partition coefficients between 0 and 15 GPa along the peridotite solidus temperature, peridotite liquidus temperature, and corresponding melt fraction F temperatures by using the thermodynamic approach described above. Melt fraction F is included because as is suggested by the batch melting equation [21], a rising melt fraction F leads to a decrease in the total amount of incompatible trace elements in the melt. Therefore, we arranged the melt fractions in $F = 0.2$ increments while neglecting the extraction of the melt, by using

$$F(P,T) = \frac{T - T(P)_{sol}}{T(P)_{liq} - T(P)_{sol}}. \quad (11)$$

The solidus T_{sol} and liquidus temperatures T_{liq} equations which we used [22] are third-order fits to experimental data [23][24]:

$$\begin{aligned}T_{sol,ini} = & \\ & 1409K + 134.2\frac{K}{GPa} \cdot P \\ & - 6.581\frac{K}{GPa^2} \cdot P^2 + 0.1054\frac{K}{GPa^3} \cdot P^3, \end{aligned} \quad (12)$$

$$\begin{aligned}T_{liq,ini} = & \\ & 2035K + 57.46\frac{K}{GPa} \cdot P \\ & - 3.487\frac{K}{GPa^2} \cdot P^2 + 0.0769\frac{K}{GPa^3} \cdot P^3. \end{aligned} \quad (13)$$

For pressures from 0-15 GPa, the solidus temperatures range from 1409-2297 K, while the liquidus temperatures go from 2035-2372 K. The pressure step size for each temperature profile is 0.1 GPa, which corresponds to 151 D_{Na}-P-T data points for each melt temperature profile. With the least square function, these data points were fitted to a function with parameters a, b, c, d, e, and f (14) in Python 3. Because the function has the same form as the fit function of Blundy et al. (1995) [13], their fit parameters are compared in Table II.

$$\begin{aligned}&\mathrm{D}_{Na}(\mathrm{T[K],P[GPa]}) = \\ &\exp\left(\frac{a + b \cdot P - c \cdot P^2}{T} - d + e \cdot P - f \cdot P^2\right). \end{aligned} \quad (14)$$

TABLE I
THERMODYNAMIC INPUT DATA FOR LIQUID AND SOLID JADEITE AND COMPARISON OF MODEL PARAMETERS.

Parameters	Pyroxene	Melt	Units
V^0	60.4	79.9	kJ GPa^{-1}
α^0	2.81·10^{-5}	6.28·10^{-5}	K^{-1}
K_T	141.2[b]	14.8	GPa
$\partial K/\partial T$	-0.025	-0.0015	GPa K^{-1}
K'	4.5	4.5	
$\Delta H_{f(0.1,T_f)}$	61.1±1.3		kJ mol^{-1}
$\Delta S_{f(0.1,T_f)}$	64.8±0.6		J mol^{-1}
T_f	943±22		K
C_p			
1	0.30113	0.28995[a]	kJ mol^{-1} K^{-1}
2	1.0143· 10^{-5}		kJ mol^{-1} K^{-1}
3	-2239.3		kJ mol^{-1} K^{-1}
4	-2.0551		kJ mol^{-1} K^{-1}

Parameters as in Blundy et al. (1995) [13] at 0.0001 GPa and 298 K (unless stated otherwise).
[a] At temperatures >1200 K.
*$C_p = C_{p1} + C_{p2} \cdot T + C_{p3} \cdot T^{-2} + C_{p4} \cdot T^{-0.5}$ (T in kelvins)

By including the melt fraction P-T profiles, we make sure that the resulting model function will satisfy a broader range of P-T conditions and is not only valid for modelling partial melting in the mantle (where temperatures are close to the solidus), but also for crystallisation of melt (where temperatures are close to the liquidus). In contrast to our model, partition coefficients for crystallising liquid were often determined by taking only the liquidus temperatures into account [25][26][27].

For both, the thermodynamic model and the fit function development, replication data is accessible in the TRR170-DB [28].

III. Results

A. Thermodynamic Model Along Melting Temperature Profiles

In a pressure range between 0 and 15 GPa and a temperature range between 1400 and 2400 K, the thermodynamic model produces increasing partition coefficients from low P/high T (0 GPa/2400 K) to high P/low T (10-12 GPa/1400 K) conditions (Figure. 2). The increase is in the order of four magnitudes and coincides with experimental observations [29][30]. At higher pressure above 12 GPa and low temperatures, the model starts to invert the trend and the partition coefficients decrease with increasing pressure. However, for our fit function development we have used the P-T space between the solidus and liquidus, which is not affected by this inversion. Along the melting temperature profiles, increasing pressure always leads to increasing partition coefficients, while increasing temperatures cause the partition coefficients to decrease (Figure 2).

In Table II, we compare the thermodynamic model results with experimental literature data. It is notable that most of the experimental data fit well to the model results. On average, the coefficients calculated by the thermodynamic model deviate from the experimental data by 26%. The best fitting value deviates only 2.9% from the experiments at 0.0001 GPa and 1526 K, while the worst fit deviates by 46.9% at 0.0001 GPa and 1524 K. The implications of this variance will be discussed in section IV.

B. Parametrisation of Thermodynamic Model Results

As described in section II-B, we developed a scaled equation along the mantle peridotite solidus, liquidus, and corresponding melt fraction temperatures in between. For this, we used the least square function to fit the thermodynamic model results presented in Figure 2 to the following equation:

$$\mathrm{D}_{Na}(\mathrm{T[K]},\mathrm{P[GPa]}) = \exp\left(\frac{2183 + 2517P - 157P^2}{T} - 4.575 - 0.5149P + 0.0475P^2\right). \quad (15)$$

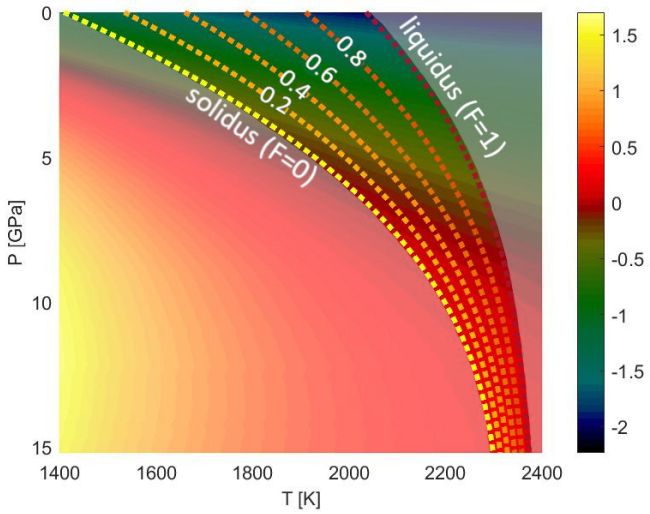

Figure 2. Sodium in clinopyroxene partition coefficients in P-T space, calculated thermodynamically with the methods of Blundy et al (1995) [13]. Solidus 12, liquidus (13) and intermediate melt fraction outlines are calculated from de Smet (1999) [22].

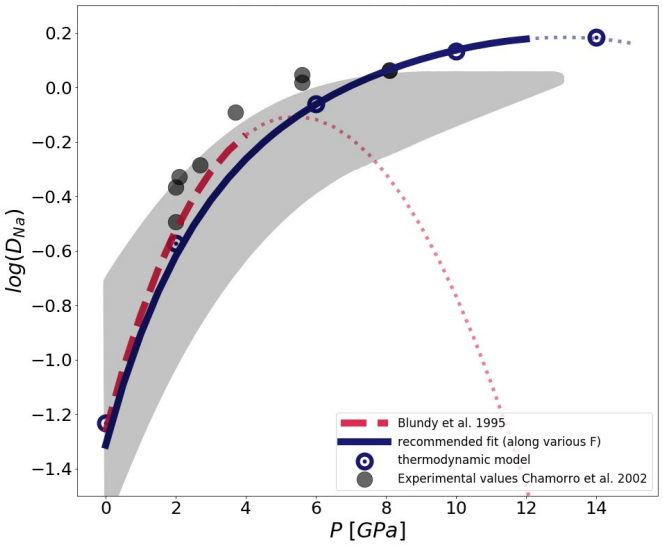

Figure 3. D_{Na} fits along the solidus from Blundy et al. (1995) [13] (red, dashed line) and this study (blue, solid line) compared to experimental data [30] (shaded grey area and grey dots) for comparison. Thin dotted lines are extrapolations of the fit functions beyond range of validity.

With the new resulting scaling law (15), it is now possible to calculate partition coefficients for sodium at varied temperature and pressure conditions.

Figure 3 illustrates how the rising D_{Na} values correlate with rising pressure along the solidus temperature. In contrast to the fit function of Blundy et al. (1995) [13], our resulting function produces steadily rising values up to 13.2 GPa at the respective peridotite solidus temperatures. After this point, the calculated values are starting to decrease. In contrast to our study, the model values of Blundy et al. (1995) [13]

 ISBN: 978-1-61208-871-6

TABLE II
COMPARISON OF EXPERIMENTAL DATA FOR CLINOPYROXENE/MELT PARTITION COEFFICIENTS WITH THE THERMODYNAMIC DATA

P [GPa]	T [K]	D_{Na} (experimental data)	Ref.	therm. model (this study)	Fit values by Blundy et al. (1995) [13]	Fit (this study)
0.0001	1370	0.050(4)	[13]	0.0696	0.0670	0.0507*
0.0001	1449	0.042(4)	[13]	0.0496	0.0444	0.0465*
0.0001	1524	0.070(19)	[13]	0.0372	0.0312	0.0432*
0.0001	1526	0.040(4)	[13]	0.0369	0.0309	0.0431*
0.0001	1526	0.038(5)	[13]	0.0369	0.0309	0.0431*
0.0001	1598	0.046(5)	[13]	0.0288	0.0228	0.0404*
1	1663	0.075(7)	[13]	0.0891	0.0794	0.0991*
2	1773	0.113(8)	[13]	0.1708	0.1680	0.1827*
2	1843	0.144(13)	[13]	0.1363	0.1247	0.1587*
3	1938	0.237(30)	[13]	0.2241	0.2170	0.2465*
6	2038	0.52(12)	[13]	0.7789	0.6507*	0.7774
1.2	1588	0.225(5)	[31]	0.1497	0.1494	0.1366*
1.2	1458	0.221(5)	[31]	0.2671	0.3039	0.1807*
1.6	1643	0.283(4)	[31]	0.1866	0.1927	0.1750*

Parameter	Fit [13] 0-4 GPa	Fit (this study) 4-12 GPa
a	10367	2183
b	2100	2517
c	165	-157
d	-10.27	-4.575
e	0.358	-0.5149

D_{Na} is the experimentally determined weight partition coefficient.
*Note that these are extrapolated values (beyond valid P-T range).
Parameters to be inserted into (14).

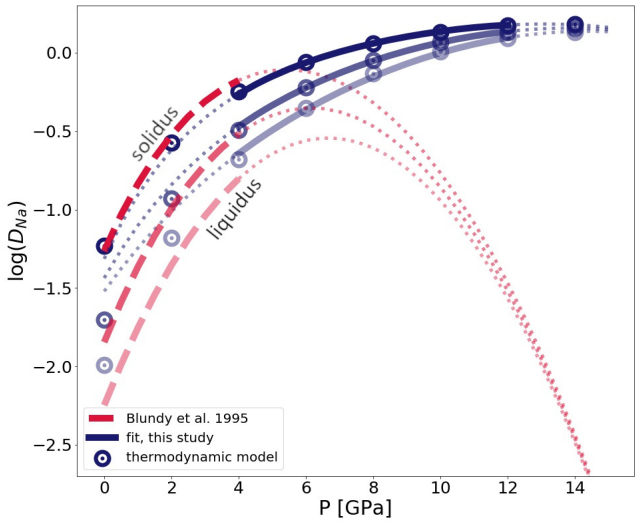

Figure 4. Partition coefficients depending on melt fractions. The line in between liquidus and solidus indicates a melt fraction F=0.5. Thin dotted lines are extrapolations of the fit functions beyond range of validity.

start to decline after approximately 5 GPa along the solidus temperature. However, Blundy et al. (1995) [13] themselves state that their scaling law is not to be used over a pressure of 4 GPa.

In Figure 4, the decrease of partition coefficients from the solidus towards the liquidus becomes visible. This indicates that not only pressure, but also temperature and therefore melt fractions have an impact on the redistribution. It should be noted that at low pressures and high melt fractions, our fit seems to divert more from the thermodynamic model than the previous fit [13]. Consequences of this diversion on the applicability of our scaling law (15) are explored in section IV.

IV. DISCUSSION

Partition coefficients are highly controlled by pressure, temperature, and composition. Since it is not possible for models to include all compositional interactions between a mineral and melt, comparing them to experimental data is sometimes difficult. This is especially true for higher pressures, where partition coefficient data is, to this date, often lacking. However, the existing experimental data for lower pressures already indicate if we can expect realistic results from our calculations. As is shown in Table II, our thermodynamic model results fit well to the experimental results [13][31]. Best matches were achieved for experimental data at 0.0001 GPa/1526 K, 2 GPa/1843 K and 3 GPa/1938 K [13], where the model data deviates from the experimental values by only 2.9% and for the latter two by 5.4%, respectively. Interestingly, with 46.9%, the second largest diversion from the experimental data is at 0.0001 GPa/1524 K, which is at the same pressure and only 2 K below a very well fitting value (Table II). However, the experimentally derived partition coefficients vary more than what could be solely explained by changing P-T conditions. Deviating experimental and thermodynamic model results can happen

 ISBN: 978-1-61208-871-6

because of several effects. For example, analytical error margins have to be considered. Furthermore, the composition of melt as well as solid clinopyroxene can be much more diverse in experiments than it is for thermodynamic model calculations, which does not take these changes into account.

It should be noted that the fit parameters in (14) differ from the parametrisation in Blundy et al. (1995) [13], which is due to the larger parameter space applied in our model. For a comparison of the two scaling laws, we refer to Figure 3 and Figure 4. A direct comparison of the resulting parameters for the scaling law of our and the previous study [13] is given in Table II.

Figure 3 illustrates that the partition coefficients calculated with our scaling law (15) over solidus temperatures is close to the experimental sodium partitioning data. This data is indicated by a shaded grey area and, for D_{Na} in the $Ab_{80}Di_{20}$ system, by darker grey dots [30]. A direct comparison with appropriate temperatures in the range of the experimental data [30] shows that here, the thermodynamic model is within an error of on average 32%.

As is shown in Figure 3 and Figure 4, our and the previous fit [13] do not completely agree with each other. Blundy et al. (1995) [13] parametrised their thermodynamically calculated results over a peridotite solidus of McKenzie and Bickle (1988) [32], while we took the peridotite solidus equation of de Smet (1999) [22]. This could have produced a small shift in the D_{Na}-P-T field and, therefore, in the resulting fit function. Also, a different parametrisation method could have been used by the previous study [13], which might have produced slightly different fits. Finally, the previous study [13] concentrated more on low pressure partitioning, whereas we have tried to parametrise the function up to the 410 km discontinuity. The inclusion of higher pressures could also be the reason why at pressures below 4 GPa (especially at higher melt fractions) our scaling law (15) fits less well to the thermodynamic model values than the older model [13].

Between 4 and 12 GPa, our scaling law (15) fits well to the thermodynamic data over all melt fraction values from solidus to liquidus. However, at high melt fractions below 4 GPa, larger diversions from the original fit function [13] appear (Figure 4). The reason for this lies in the nature of the least square parametrisation used in Python 3, which allows the fit function to divert from the thermodynamic model at low pressures for the expense of being applicable to higher pressures and to a wide range of melt fractions. If we would only parametrise the model over the solidus, the shift would disappear at the expense of the model being applicable to any other P-T conditions. Thus, the included P-T conditions for the varying melt fractions ensure that the model is useful over a wide range of pressures and temperatures, but limits the applicability of the scaling law for higher melt fractions to a range between 4 and 12 GPa.

In the upper mantle, buoyant melt can occur up to the depth where it becomes gravitationally stable and a density inversion of melt and solid surrounding material takes place (the so-called density crossover). In other words, melts formed at higher pressures may not be able to rise to the surface [33][34]. However, this is only true for upper mantle melts and melts rising upwards in lower regions of the Earth can not be ruled out [35]. Inside Earth, the density crossover exists at approximately 11-12 GPa at 2000°C [36], and in Mars between 7 GPa [36] and 7.5 GPa [37]. To include pressure and temperature dependent partition coefficients into a mantle evolution model, it would often suffice to be able to calculate them up to the density crossover. Overlapping with the density crossover, in the Earth's 410 km mantle discontinuity (i.e., pressures of approximately 12-15 GPa), phase changes occur [38] and pyroxene slowly starts to dissolve into a pyrope-rich garnet to form majorite [39]. This and the density crossover indicate that a parametrisation up to approximately 12-15 GPa is sufficient.

As the experimental data [30][29] suggests, the partition coefficients of sodium in clinopyroxene increase with temperature and pressure before they remain constant. At solidus P-T conditions, our fit function curve slowly starts to flatten and starts to fall at approximately 13 GPa (Figure 3). This coincides with the thermodynamic model, where (along the solidus) the partition coefficients start to decrease at 12.5 GPa. Combining these findings with the occurence of a density crossover and transition zone at approximately 12 GPa, we suggest to not use our scaling law (15) above this pressure.

As is discussed above, the scaling law works well for melting P-T conditions between the peridotite solidus and liquidus between 4 and 12 GPa. Thus, it can be considered as a useful expansion of the previous scaling law for D_{Na} [13]. Because of the broad P-T range, the model should not only be useful for mantle melting, but also for models which crystallise melt, as is the case in a magma ocean. However, as recent studies have suggested, the solidus and liquidus temperature may change heavily depending on if material is melting or crystallising [40]. If this is the case, our model could lie outside of the P-T range between solidus and liquidus for crystallising liquids and would have to be extrapolated. Therefore, one has to be careful with the usage of the fit.

Like the thermodynamic model, phase transitions and density crossover behavior all depend on pressure. Thus, even for planets with a radius or mass different from Earth, the fit should be applicable if the mantle composition is comparable to Earth. Additionally, the composition of the terrestrial planet has to be taken into account. If there is no or if there are only very minor portions of clinopyroxene in the planets upper mantle, our partition coefficient calculations for clinopyroxene cannot be used.

V. Conclusion and Future Work

With the new high-pressure scaling law (15), it is now possible to include partition coefficient models depending on pressure and temperature into mantle convection models for the entire pressure range over which upper mantle melts are

buoyant. The newly developed fit function can be used to calculate clinopyroxene/melt redistribution behavior of sodium starting from 4 GPa up to the mantle transition zone of the Earth. This is in contrast to the scaling law by Blundy et al. (1995) [13], which can be applied from 0 to 4 GPa. Our new scaling law can be used as the basis for calculating D_i in (1), with D_0=D_{Na} for 1+ charge elements. Possible approaches to model partition coefficients based on this scaling law for the charges 2+ to 4+ are described in Wood and Blundy (2014) [41] and are based on adjusted calculations for the mineral's lattice site radius r_0 and the bulk modulus E.

Compared to the existing experimental data, our scaling law (15) allows for a good approximation of clinopyroxene partition coefficients of trace elements between solid and melt. This enables us to do self-consistent calculations of local partition coefficients for variable pressures and temperatures. Because we have parametrised our model over a wide range of P-T conditions and melt fractions between the peridotite solidus and liquidus, our model can be applied for any $D_{Na}^{cpx/melt}$ calculation between 1850-2360 K and 4-12 GPa.

By combining our scaling law with the older scaling law [13], we will be able to calculate the redistribution behavior of trace elements in terrestrial planets in much more detail. Our partition coefficient calculations for clinopyroxene should be applicable as long as clinopyroxene is present in the planet's upper mantle in sufficient abundance.

Future works could not only include the application of our new scaling law (15) in numerical simulations, but also further investigations on partitioning behavior in mantle material as well. For instance, adding an orthopyroxene/melt trace element partitioning model to a mantle evolution model would provide an even more detailed tool to study on the trace element redistribution from mantle to crust if used alongside the clinopyroxene/melt partitioning model.

ACKNOWLEDGMENT

We would like to thank Jon Blundy and Timm John for fruitful discussions on partition coefficient modelling. This study was funded by the Deutsche Forschungsgemeinschaft (DFG, German Research Foundation) – Project-ID 263649064 – TRR 170. This is TRR 170 Publication No. 130.

REFERENCES

[1] H. Neumann, J. Mead, and C. Vitaliano "Trace element variation during fractional crystallization as calculated from the distribution law," Geochimica et Cosmochimica Acta, vol. 6 (2-3), pp. 90-99, February 1954.

[2] P. W. Gast "Trace element fractionation and the origin of tholeiitic and alka-line magma types," Geochimica et Cosmochimica Acta, vol. 32 (10), pp. 1057-1086, October 1968.

[3] B. B. Jensen "Patterns of trace element partitioning," Geochimica et Cosmochimica Acta, vol. 37 (10), pp. 2227-2242, October 1973.

[4] K. T. Johnson, H. J. Dick, and N. Shimizu "Melting in the oceanic upper mantle: an ion microprobe study of diopsides in abyssal peridotites," Journal of Geophysical Research: Solid Earth, 95 (B3), 2661-2678, March 1990.

[5] T. Skulski, W. Minarik, and E. B. Watson, E. B. "High-pressure experimental trace-element partitioning between clinopyroxene and basaltic melts," Chemical Geology, vol. 117 (1-4), pp. 127-147, November 1994.

[6] U. Walzer, and R. Hendel "Mantle convection and evolution with growing continents" Journal of Geophysical Research: Solid Earth, vol. 113 (B9), September 2008.

[7] A. Morschhauser, M. Grott, and D. Breuer "Crustal recycling, mantle dehydration, and the thermal evolution of Mars," Icarus, vol. 212 (2), pp. 541-558, April 2011.

[8] T. Ruedas, P. J. Tackley, and S. C. Solomon "Thermal and compositional evolution of the martian mantle: Effects of phase transitions and melting," Physics of the Earth and Planetary Interiors, vol. 216 , pp. 32-58, March 2013.

[9] A.-C. Plesa, and D. Breuer "Partial melting in one-plate planets: Implications for thermo-chemical and atmospheric evolution," Planetary and Space Science, vol-405 98 , pp. 50-65, August 2014.

[10] R. E. Jones, P. E. van Keken, E. H. Hauri, J. M. Tucker, J. Vervoort, and C. J. Ballentine "Origins of the terrestrial Hf-Nd mantle array: evidence from a combined geodynamical-geochemical approach," Earth and Planetary Science Letters, vol. 518 , pp. 26-39, July 2019.

[11] V. M. Goldschmidt "The principles of distribution of chemical elements in minerals and rocks," Journal of the Chemical Society (Resumed), pp. 655-673, March 1937.

[12] J. Brice "Some thermodynamic aspects of the growth of strained crystals," Journal of Crystal Growth, vol. 28 (2), pp. 249-253, March 1975.

[13] J. Blundy, T. Falloon, B. Wood, and J. Dalton "Sodium partitioning between clinopyroxene and silicate melts," Journal of Geophysical Research: Solid Earth, vol. 340 100 (B8), pp. 15501-15515, August 1995.

[14] J. M. Schmidt and L. Noack "Modelling clinopyroxene/melt partition coefficients for higher upper mantle pressures," EGU General Assembly 2021, online, EGU21-12478, https://doi.org/10.5194/egusphere-egu21-12478, April 2021.

[15] P. McDade, J. D. Blundy, and B. J. Wood "Trace element partitioning on the Tinaquillo Lherzolite solidus at 1.5 GPa," Physics of the Earth and Planetary Interiors, vol. 139 (1-2), pp. 129-147, September 2003.

[16] B. J. Wood, and J. Nicholls "The thermodynamic properties of reciprocal solid solutions," Contributions to Mineralogy and Petrology, vol. 66 (4), pp. 389-400, June 1978.

[17] J. Blundy, and B. Wood "Crystal-chemical controls on the partitioning of Sr and Ba between plagioclase feldspar, silicate melts, and hydrothermal solutions," Geochimica et Cosmochimica Acta, vol. 55 (1), pp. 193-209, January 1991.

[18] B. J. Wood, and J. D. Blundy "A predictive model for rare earth element partitioning between clinopyroxene

and anhydrous silicate melt," Contributions to Mineralogy and Petrology, vol. 129 (2-3), pp. 166-181, October 1997.

[19] K. Grjotheim, C. Krohn, and J. Toguri "Thermodynamic evaluation of activities in molten mixtures of reciprocal salt systems," Transactions of the Faraday Society, vol. 57 , pp. 1949-1957, March 1961.

[20] C. G. Maier, and K. Kelley "An equation for the representation of high-temperature heat content data," Journal of the American chemical society, vol. 54 (8), pp. 3243-3246, August 1932.

[21] J. Hertogen, and R. Gijbels "Calculation of trace element fractionation during partial melting," Geochimica et Cosmochimica Acta, vol. 40 (3), pp. 313-322, March 1976.

[22] J. De Smet, A. Van Den Berg, and N. Vlaar, N. "The evolution of continental roots in numerical thermo-chemical mantle convection models including differentiation by partial melting," In: Developments in geotectonics. Elsevier, vol. 24, pp. 153-170, 1999.

[23] T. Gasparik "Phase relations in the transition zone," Journal of Geophysical Research: Solid Earth, vol. 95 (B10), pp. 15751-15769, September 1990.

[24] E. Takahashi "Speculations on the Archean mantle: missing link between komatiite and depleted garnet peridotite," Journal of Geophysical Research: Solid Earth, vol. 95 (B10), pp. 15941-15954, September 1990.

[25] D. C. Presnall, Y.-H. Weng, C. S. Milholland, and M. J. Walter "Liquidus phase relations in the system MgO-MgSiO3 at pressures up to 25 GPa - constraints on crystallization of a molten Hadean mantle," Physics of the Earth and Planetary Interiors, vol. 107 (1-3), pp. 83-95, April 1998.

[26] M. Walter, E. Nakamura, R. Tronnes, R., and D. Frost, D. "Experimental constraints on crystallization differentiation in a deep magma ocean," Geochimica et Cosmochimica Acta, vol. 68 (20), pp. 4267-4284, October 2004.

[27] D. M. Shaw "Trace element fractionation during anatexis," Geochimica et Cosmochimica Acta, vol. 34 (2), pp. 237-243, February 1970.

[28] J. M. Schmidt, and L. Noack "Replication Data for Parameterizing a Model of Clinopyroxene/Melt Partition Coefficients for Sodium to Higher Upper Mantle Pressures," TRR170-DB doi.org/10.35003/QVOL83 (V01), 2021.

[29] W. Wang, and E. Takahashi "Subsolidus and melting experiments of a K-rich basaltic composition to 27 GPa: Implication for the behavior of potassium in the mantle," American Mineralogist , vol. 84 (3), pp. 357-361, November 1999.

[30] E. Chamorro, R. Brooker, J. A. Wartho, B. Wood, S. Kelley, and J. Blundy "Ar and K partitioning between clinopyroxene and silicate melt to 8 GPa," Geochimica et Cosmochimica Acta, vol. 66 (3), pp. 507-519, February 2002.

[31] G. A. Gaetani, A. J. Kent, T. L. Grove, I. D. Hutcheon, and E. M. Stolper "Mineral/melt partitioning of trace elements during hydrous peridotite partial melting," Contributions to Mineralogy and Petrology, vol. 145 (4), pp. 391-405, May 2003.

[32] D. Mckenzie, and M. Bickle "The volume and composition of melt generated by extension of the lithosphere," Journal of petrology, vol. 29 (3), pp. 625-679, June 1988.

[33] E. Stolper, D. Walker, B. H. Hager, and J. F. Hays "Melt segregation from partially molten source regions: the importance of melt density and source region size," Journal of Geophysical Research: Solid Earth, vol. 86 (B7), pp. 6261-6271, July 1981.

[34] Z. Jing, and S.-i. Karato "The density of volatile bearing melts in the Earth's deep mantle: The role of chemical composition," Chemical Geology, vol. 262 (1-2), pp. 100-107, May 2009.

[35] M. J. Beuchert and H. Schmeling "A melting model for the lowermost mantle using Clapeyron slopes derived from experimental data: Consequences for the thickness of ultralow velocity zones (ULVZs)," Geochemistry, Geophysics, Geosystems, vol. 14 (1), pp. 197-208, January 2013.

[36] E. Ohtani, Y. Nagata, A. Suzuki, and T. Kato "Melting relations of peridotite and the density crossover in planetary mantles," Chemical Geology, vol. 402 120 (3-4), pp. 207-221, March 1995.

[37] L. T. Elkins-Tanton, E. Parmentier, and P. Hess "Magma ocean fractional crystallization and cumulate overturn in terrestrial planets: Implications for Mars," Meteoritics & Planetary Science, vol. 38 (12), pp. 1753-1771, January 2003.

[38] A. E. Ringwood, A. E. "Phase transformations and their bearing on the constitution and dynamics of the mantle," Geochimica et Cosmochimica Acta, vol. 55 (8), pp. 2083-2110, August 1991.

[39] M. Akaogi "Phase transitions of minerals in the transition zone and upper part of the lower mantle," Special Papers-Geological Society Of America, vol. 421 , p. 1, 2007.

[40] C.-E. Boukare, Y. Ricard, and G. Fiquet "Thermodynamics of the MgO-FeO-SiO2 system up to 140 GPa: Application to the crystallization of Earth's magma ocean," Journal of Geophysical Research: Solid Earth, vol. 120 (9), pp. 6085-6101, August 2015.

[41] B. J. Wood, and J. D. Blundy, J. D. (2014) "Trace element partitioning: The influences of ionic radius, cation charge, pressure, and temperature," In H. D. Holland and K. K. Turekian (Eds.), Treatise on geochemistry (second edition) (Second Edition ed., p. 421 - 448). Oxford: Elsevier, 2014.

 ISBN: 978-1-61208-871-6